A Cluster Algorithm for Gross-Neveu Fermions at Nonzero Temperature

by

Sarah Maureen Harrison

Submitted to the Department of Physics
in partial fulfillment of the requirements for the degree of

Bachelor of Science in Physics

at the

MASSACHUSETTS INSTITUTE OF TECHNOLOGY

June 2009

Author .....
Department of Physics
May 8, 2009

Certified by .....
Krishna Rajagopal
Professor
Thesis Supervisor

Accepted by .....
David E. Pritchard
Senior Thesis Coordinator, Department of Physics

A Cluster Algorithm for Gross-Neveu Fermions at Nonzero Temperature

by

Sarah Maureen Harrison

Submitted to the Department of Physics
on May 8, 2009, in partial fulfillment of the
requirements for the degree of
Bachelor of Science in Physics

Abstract

In this thesis we present results of lattice simulations of Gross-Neveu fermions in $1+1$ dimensions. We rederive the representation of N flavors of Wilson fermions in terms of Ising spins on a $1+1$ dimensional lattice from [1]. We reimplement the cluster algorithm of [1] for N flavors of free fermions and verify it against exact monomer densities in the free theory. In addition, we extend this algorithm to the interacting case using the prescription outlined in [1] and produce results for fermion correlation functions in the Gross-Neveu model using a cluster algorithm for the first time. To analyze Gross-Neveu fermions at nonzero temperature, we develop an algorithm to simulate fluctuating boundary conditions. We calculate the chiral condensate at nonzero temperature using this algorithm and see evidence consistent with a phase transition in the large N limit.

Thesis Supervisor: Krishna Rajagopal
Title: Professor

Acknowledgments

I would like to thank Dr. Harvey Meyer, who helped me a great deal with understanding the science of this project. I would also like to thank Professor Krishna Rajagopal for his incredible guidance and support.

Contents

List of Figures

List of Tables

Chapter 1

Introduction

1.1 Cluster Algorithms for Efficient Monte Carlo Simulations

When studying systems with large numbers of degrees of freedom, it is useful to treat these systems numerically on the computer, as it is often impossible to directly compute the partition function,

$$Z = \sum_{states} e^{-\beta H} \tag{1.1.1}$$

where β is the inverse temperature and H is the energy of the system. Instead, one can use Monte Carlo methods to randomly generate configurations of the system which have a high Boltzmann weight. In this case the partition function can be approximated as a suitably weighted sum over these randomly generated most probable states. Since expectation values of thermodynamic quantities are integrals over all possible states weighted by the Boltzmann distribution, we can also use these methods to calculate values of physical observables.

As an example, consider the Ising model in two dimensions. The Ising model is a collection of particles which lie on discrete lattice sites and which have a single property called spin that can take on values $+1$ or -1. The energy of the system is

derived from each particle's interaction with its nearest neighbors. The Hamiltonian for the Ising model is

$$H = -J \sum_{\langle ij \rangle} s_i s_j \tag{1.1.2}$$

where $J > 0$ is a constant, $\langle ij \rangle$ denotes nearest neighbor lattice sites, s_i is the value of the spin at lattice site i, and $s_i \in \{\pm 1\}$. From this, we can see that adjacent particles with the same spin contribute negatively to the energy of the system and those with opposite spin contribute positively.

The order parameter for the Ising model is the magnetization

$$M = \left| \frac{1}{N} \sum_i s_i \right| \tag{1.1.3}$$

or the absolute value of the average spin per lattice site, where N is the total number of particles. At $T = 0$, the lowest energy state is the state where all spins take on the same value, and $M = 1$. Because there are two possible lowest energy states, one with all spins taking on the value $+1$ and one with all spins taking on the value -1, the global spin flip symmetry ($s_i \rightarrow -s_i$) of the Hamiltonian is spontaneously broken in either of the two ground states. At very high temperature however, the equilibrium state is a disordered state with $M = 0$. At a critical temperature T_c, the system transitions from a state of spontaneously broken spin flip symmetry (characterized by a nonzero magnetization) to a state where the symmetry is restored (and $M = 0$). In order to study the properties of this phase transition using Monte Carlo techniques, we would like to have a method to compute the average magnetization of the system as a function of temperature.

For an Ising model with N particles, there are 2^N possible states, and thus it is not practical to directly compute the average magnetization for this system. Instead, we would like to do so using only the most probable configurations, or those configurations where the Helmholtz free energy ($F = -\frac{1}{\beta} \ln Z$) is minimized. The simplest algorithms to randomly generate most probable configurations are local updating algorithms. One example of this type of algorithm is the Metropolis algorithm. During

one iteration of the algorithm, the program visits each lattice site and calculates whether the energy is made smaller if the spin at that lattice point is flipped. If $\Delta H \leq 0$, the spin is flipped with probability 1, and if not, the spin is flipped with probability proportional to $e^{-\beta \Delta H}$ where β is the inverse temperature. The system evolves through computer time toward an equilibrium configuration. The drawback of the Metropolis algorithm and similar algorithms is they have a high autocorrelation times. That is, the number of iterations of the algorithm over which configurations are correlated is significant.

Cluster algorithms provide dramatic improvements on these local updating algorithms. Instead of flipping one spin at a time, cluster algorithms flip whole groups of lattice sites at once. Among the earliest cluster algorithms that were developed are those of Swendsen and Wang for the two dimensional Potts model [3] and Wolff for $O(n)$ models in two dimensions [4]. A sketch of a cluster algorithm of this type for the case of the Ising model is as follows.

1. Choose a random spin on the lattice to be the first spin in a cluster.

2. Visit each of its nearest neightbors, and if the value of an adjacent spin is the same, then include it in the cluster with probability $p = 1 - e^{-2\beta}$. If the adjacent point has opposite spin, do not include it in the cluster.

3. Visit the nearest neighbors of each of the newly added spins and continue growing the cluster in this way until no more spins are added.

4. Flip the value of all of the spins in the cluster.

These steps will generate one new lattice configuration. Because many spins are updated at once, algorithms of this type greatly decrease relaxation times and autocorrelations.

When simulating phase transitions, we run into difficulty because of long correlation times at and around the critical point. Cluster algorithms have the advantage of greatly reducing the effect of critical slowing down. This allows simulations at increased lattice sizes, which leads to the reduction of finite-size effects. In this paper

we develop and implement a cluster algorithm to study the properties of Gross-Neveu model fermions.

1.2 The Gross-Neveu Model

The Gross-Neveu model is a theory of relativistic fermions in $1+1$ dimensions (one space and one time dimension) with a four-fermion interaction. This model is both renormalizable and asymptotically free, and because of its simplicity was created to study the properties of more complex asymptotically free theories, such as QCD. The original action described by Gross and Neveu [5] is

$$S = \int d^2x \left[\bar{\psi}(x) i \not{\partial} \psi(x) + \frac{1}{2} g^2 (\bar{\psi}(x)\psi(x))^2 \right] \tag{1.2.1}$$

where ψ is a massless fermion field with two spinor indices and N flavor indices. This action is invariant under the chiral transformation

$$\psi \rightarrow \gamma_5 \psi. \tag{1.2.2}$$

Spontaneous symmetry breaking of this chiral symmetry results in a nonzero value of the fermion condensate $\langle \bar{\psi}\psi \rangle$ and causes the generation of a fermion mass, which was described in [5].

For the computational tools we develop in this paper, it will be most convenient to write the Gross-Neveu action in terms of Majorana fermions, as presented in [1]. A Majorana fermion, which is its own antiparticle, will be represented by a Grassman-valued field ξ_i with two spin components. One Dirac fermion can be written as a combination of two species of Majorana fermions as

$$\psi = \frac{1}{\sqrt{2}}(\xi_1 + i\xi_2) \tag{1.2.3}$$

$$\bar{\psi} = \frac{1}{\sqrt{2}}(\xi_1 - i\xi_2)^\top C. \tag{1.2.4}$$

From this, we can see that a theory with N flavors of Dirac fermions corresponds to

a theory with $2N$ flavors of Majorana fermions.

We will use Wilson's method for representing fermions on a lattice, which corresponds to replacing the mass term

$$m\bar{\psi}(x)\psi(x) \to m\bar{\psi}(x)\psi(x) - \frac{r}{2}\partial_\mu\bar{\psi}(x)\partial_\mu\psi(x). \tag{1.2.5}$$

The Wilson discretization of equation (1.2.1) where we set $r = 1$ (as in [1]) written in terms of Majorana fermions is given by

$$S = \sum_x \left[\frac{1}{2}\xi^\top C(\gamma_\mu\tilde{\partial}_\mu + m - \frac{1}{2}\partial^*\partial)\xi - \frac{g^2}{8}(\xi^\top C\xi)^2\right] \tag{1.2.6}$$

where ∂, ∂^*, and $\tilde{\partial}$ are the forward, backward, and symmetric discrete derivatives on the lattice which act as

$$\begin{aligned} \partial\xi &= \xi(x+\hat{\mu}) - \xi(x) \\ \xi^\top\partial^* &= \xi^\top(x+\hat{\mu}) - \xi^\top(x) \\ \tilde{\partial}_\mu\xi &= \xi(x+\hat{\mu}) + \xi(x-\hat{\mu}) - 2\xi(x) \end{aligned} \tag{1.2.7}$$

and C is an antisymmetric matrix such that $C\gamma_\mu C^{-1} = -\gamma_\mu^\top$. The Wilson term (proportional to $\partial^*\partial$) breaks the discrete chiral symmetry $\xi \to \gamma_5\xi$ of the massless theory. This symmetry is restored in the continuum limit at a critical nonzero value of the mass parameter m, which will cancel the chiral symmetry breaking effect of the Wilson term, restoring the massless form of the theory.

The partition function for one free Majorana fermion on a lattice with definite boundary conditions ϵ is

$$Z_\xi^\epsilon[m] = \int D\xi e^{-S_{free}} = Pf[C(\gamma_\mu\tilde{\partial}_\mu + m - \frac{1}{2}\partial^*\partial)] \tag{1.2.8}$$

where S_{free} is the action from equation (1.2.1) with $g = 0$ and Pf denotes the pfaffian. The partition function for N flavors of free Majorana fermions is just $(Z_\xi^\epsilon[m])^N$. If we consider the mass parameter as x-dependent, $m = m(x)$, then we can write the full

partition function for the Gross-Neveu model with N flavors of fermions in terms of derivatives with respect to $m(x)$ acting on the N-flavor free partition function [1] as

$$Z_{GN} = \int D\xi e^{-S} = \exp\left\{\frac{g^2}{2}\sum_x \frac{\partial^2}{\partial m(x)^2}\right\}(Z_\xi^\epsilon[m])^N. \tag{1.2.9}$$

There are four possibilities for the ϵ of equation (1.2.8). On a two dimensional lattice with T lattice sites in the time direction and L lattice sites in the space direction, thepossible choices of boundary condition are $\epsilon = (\epsilon_T, \epsilon_L)$ with $\epsilon_T, \epsilon_L \in \{0, 1\}$, where 0 indicates periodic boundary conditions and 1 indicates antiperiodic boundary conditions.

1.3 Fermion Phase Transitions in $1+1$ Dimensions

The properties of Gross-Neveu fermions at nonzero temperature have been studied in [6], [7], and [8]. What has been found is that at zero temperature, spontaneous symmetry breaking of the chiral symmetry causes the generation of a nonzero fermion mass. If we rewrite equation (1.2.1) as

$$S = \int d^2x \left[\bar{\psi} i \not{\partial}\psi - \frac{1}{2g^2}\sigma^2 - \sigma\bar{\psi}\psi\right] \tag{1.3.1}$$

where σ is a scalar field, then at zero temperature, σ acquires a nonzero vacuum expectation value, $\langle\sigma\rangle = \sigma^*$ and the $\sigma\bar{\psi}\psi$ term can be interpreted as a fermion mass term. The action of equation (1.3.1) leads to the same correlation functions of the fermion fields as equation (1.2.1).

In the limit of an infinite number of flavors of fermions, it is found that at some nonzero critical temperature, T_c, the chiral symmetry is restored and the mass vanishes continuously but nonanalytically through a second order phase transition. However, for any finite N, the chiral symmetry is restored at any nonzero T due to the condensation of kinks and antikinks along the space dimension [6]. At low T, the potential of equation (1.3.1) has two symmetric minima at $\pm\sigma^*(T)$. The kinks and

antikinks are alternating segments of $+\sigma^*(T)$ and $-\sigma^*(T)$. Because of the alternation of these segments, $\langle\sigma\rangle = 0$. This means that there is only spontaneous symmetry breaking at $T = 0$ for a finite number of flavors.

In Chapter 2 we will derive two representations of fermions on the lattice–first, a loop representation originally derived by Gattringer in [2], and then a representation of Ising spins developed from the loop representation by Wolff [1]. In Chapter 3 we discuss a cluster algorithm for simulating free fermions in $1 + 1$ dimensions and present results for monomer densities for free fermions which are in agreement with exact values. We discuss the Gross-Neveu model in Chapter 4. We present a modified cluster algorithm in order to simulate interacting fermions and obtain results for the Gross-Neveu model using a cluster algorithm for the first time. We calculate fermion correlation functions at zero temperature in different boundary conditions. In Chapter 5 we study the Gross-Neveu model at nonzero temperature. We present an original algorithm for simulating fermions with fluctuating spin boundary conditions, which is necessary in order to simulate fermions at nonzero temperature. We describe results for Gross-Neveu fermions at nonzero temperature for the first time using a cluster algorithm, and demonstrate a fermion phase transition for large N. We discuss our conclusions in Chapter 6.

Chapter 2

Representing Fermions on a Computer

It is not possible to directly sample the action of equation (1.2.6) because fermionic fields are Grassman-valued. This means that we cannot sample lattice configurations of Grassman numbers because we do not have an efficient way of implementing Grassman numbers on a computer. In order to simulate fermions using Monte Carlo methods, we must first come up with a way of representing field configurations on the computer. One way of doing this is through a loop representation first described by Gattringer in [2]. He describes an equivalence between the two-dimensional Wilson fermion determinant and a sum over configurations of dimers on a lattice which form closed loops. In § 2.1 of this chapter, we rederive Gattringer's loop representation of the Gross-Neveu model. In § 2.2 we show the equivalence of this loop representation to a system of Ising spins on a lattice. In § 2.3 we discuss the extension of this spin representation to include negative values of the Gross-Neveu mass parameter. The derivations presented in this chapter follow § 3 of [1].

2.1 Rederivation of the Fermion Loop Representation

Here we will rederive the loop representation of [2] in the context of Majorana fermions with definite boundary conditions. Initially, we will ignore the four-fermion interaction term in the Gross-Neveu model and only consider the action for a free Majorana fermion in 1+1 dimensions:

$$S = \frac{1}{2}\sum_x \phi(x)\xi^\top(x)C\xi(x) - \sum_{x,\mu}\xi^\top(x)CP(\hat{\mu})\xi(x+\hat{\mu}) \tag{2.1.1}$$

where $\phi(x) = 2+m(x)$ and $P(n) = \frac{1}{2}(1-n_\mu\gamma_\mu)$ for lattice unit vectors $n = \pm\hat{\mu}$. $P(n)$ is a projection operator formed from a combination of the discrete lattice derivatives of equation (1.2.6) and has the property

$$\xi^\top(x)CP(\hat{\mu})\xi(x+\hat{\mu}) = \xi^\top(x+\hat{\mu})CP(-\hat{\mu})\xi(x). \tag{2.1.2}$$

In order to calculate observable quantities, we would like to evaluate the partition function

$$Z^\epsilon_\xi[\phi] = \int D\xi e^{-S} \tag{2.1.3}$$

where ϵ specifies a boundary condition for the ξ particles. Plugging equation (2.1.1) into equation (2.1.3), we get

$$Z^\epsilon_\xi[\phi] = \int D\xi \exp\left[-\frac{1}{2}\sum_x \phi(x)\xi^\top(x)C\xi(x) + \sum_{x,\mu}\xi^\top(x)CP(\hat{\mu})\xi(x+\hat{\mu})\right]. \tag{2.1.4}$$

We can expand the Boltzmann factor to $O(\xi^2)$ to obtain

$$Z^\epsilon_\xi[\phi] = \int D\xi \prod_x(1+\phi\xi_1(x)\xi_2(x))\prod_{x,\mu}(1+\xi^\top(x)CP(\hat{\mu})\xi(x+\hat{\mu})) \tag{2.1.5}$$

where we have used the phase convention: $-\frac{1}{2}\xi^\top C\xi = \xi_1\xi_2$. Now we reorganize this equation by introducing variables $k(x,\mu)$ which can take on values 0 or 1 and summing

over all possible configurations of $k(x,\mu)$ to obtain

$$Z_\xi^\epsilon[\phi] = \sum_{\{k(x,\mu)\}} \int D\xi \prod_x (1+\phi\xi_1(x)\xi_2(x)) \prod_{x,\mu} (\xi^\top(x) CP(\hat{\mu})\xi(x+\hat{\mu}))^{k(x,\mu)}. \quad (2.1.6)$$

These variables can be interpreted as dimers which lie on the links between lattice sites. If $k(x,\mu) = 1$, there is a dimer on the link between site x and site $x+\hat{\mu}$, and if $k(x,\mu) = 0$, there is none.

At each lattice site, there are only two possible cases which will contribute a nonzero factor to the integral in equation (2.1.6). The first case is that there are no dimers on any of the four links adjacent to x ($k(x,\mu) = 0$ for $\mu = (\pm 1, 0)$ and $\mu = (0, \pm 1)$). In this case the relevant integral is just

$$\int D\xi (1+\phi\xi_1(x)\xi_2(x)) \quad (2.1.7)$$

which contributes a factor of $\phi(x)$ to the overall weight of the configuration. These types of sites, with no adjacent links, are called monomers. Because of the properties of Grassman variables, the only other possible case is that there are two adjacent links at a particular site. Thus, there are seven types of allowed dimer configurations at a particular site, which are shown in Figure 2-1 (the second configuration shown has weight $w_2 = 0$). When we consider tiling a lattice with these types of dimer configurations, it is apparent that the only possible lattice configurations are closed loops of dimers which do not intersect or backtrack.

We want to calculate the Boltzmann weight of one of these dimer loops. Consider a loop which traverses lattice sites $(x_1, x_2, ..., x_l)$, each consecutive pair of which differs by one lattice unit vector, $\hat{n}_i$. The Boltzmann weight of this loop is given by

$$I = \int D\xi \left[\xi^\top(x_1) CP(\hat{n}_1)\xi(x_2)\right] \left[\xi^\top(x_2) CP(\hat{n}_2)\xi(x_3)\right] \ldots \left[\xi^\top(x_l) CP(\hat{n}_l)\xi(x_1)\right]. \quad (2.1.8)$$

The result of this integral is

$$I = -\mathrm{tr}[P(\hat{n}_1)P(\hat{n}_2)...P(\hat{n}_l)]. \quad (2.1.9)$$

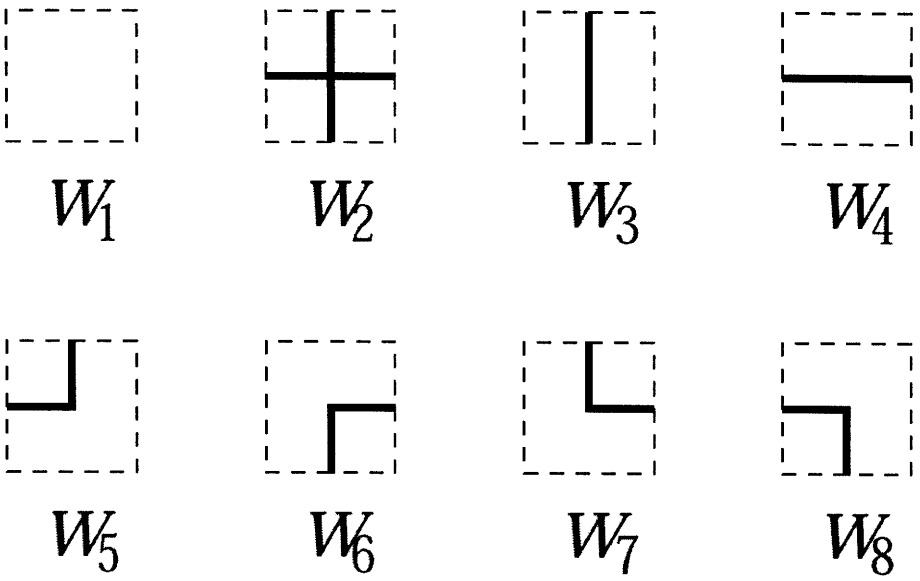

Figure 2-1: Possible configurations of dimers at each lattice site and their weights. $w_1 = \phi(x)$, $w_2 = 0$, $w_3 = w_4 = 1$, $w_5 = w_6 = w_7 = w_8 = \frac{1}{\sqrt{2}}$. The only allowed possibilities are either two dimers or zero dimers (a monomer) at a particular lattice site. This figure is taken from [2].

which can be obtained by writing the projection operators in terms of their eigenvectors as in [1]. The Boltzmann weight of the loop in terms of N_c, the number of corners it contains, and $\nu = 0, \pm 1$, the number of complete rotations it makes, is

$$I = (-1)^{\nu+1} 2^{-\frac{N_c}{2}}. \tag{2.1.10}$$

So if a loop doesn't make a full rotation ($\nu = 0$), but instead winds around the lattice then there is an extra minus sign in the weight.

Because loops can wind around the torus, we can define distinct homotopy classes of loops. Closed loops which do not wind around the lattice can be continuously reduced to a point, and thus are in the trivial homotopy class. If two loops wind around the torus in the same direction, they are also reducible to a point, and this type of configuration is still in the trivial homotopy class. However, configurations with odd numbers of loops winding in the same direction belong to distinct homotopy classes. Because loops can wind either trivially or nontrivially around the torus in each

of the two directions (time and space), there are four distinct homotopy classes of loops: $\mathcal{L}_{00}, \mathcal{L}_{01}, \mathcal{L}_{10}$, and $\mathcal{L}_{11}$, where 0 indicates an even number of loops winding in one direction (the trivial class) and 1 indicates an odd number of loops winding in one direction. Examples of configurations of loops from each homotopy class are shown in Figure 2-2. The purpose of the + and − signs in the figure will be explained in the next section.

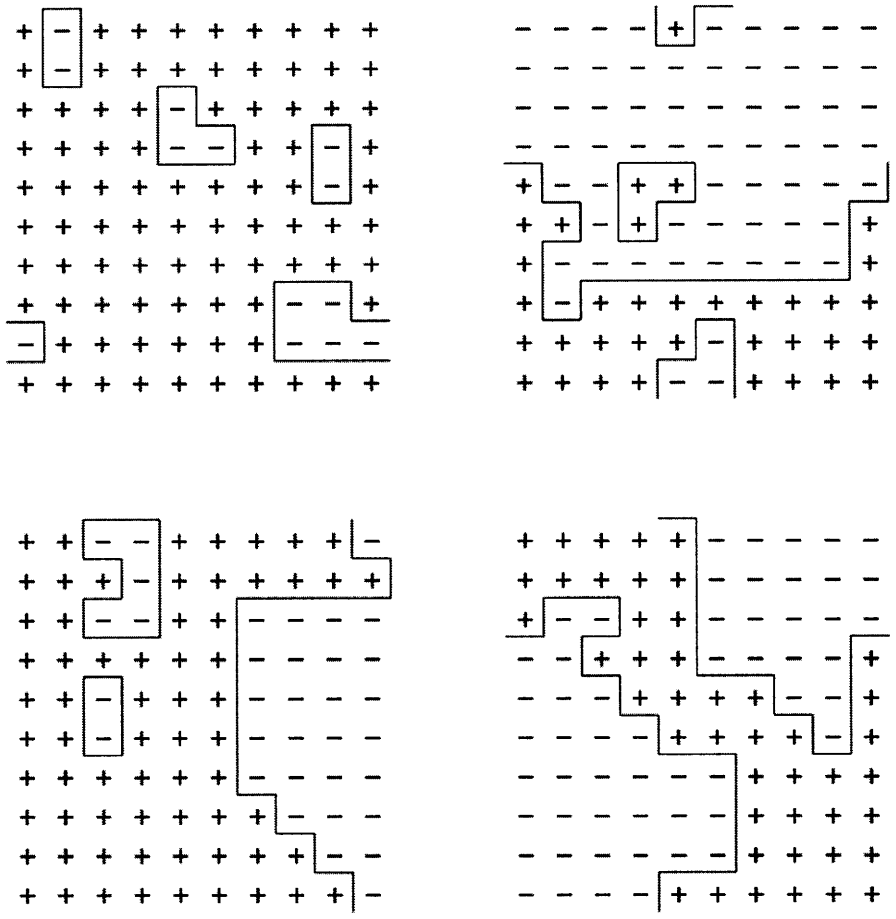

Figure 2-2: Configurations of loops in each of the four homotopy classes: $\mathcal{L}_{00}, \mathcal{L}_{10}, \mathcal{L}_{01}$, and $\mathcal{L}_{11}$, where the time direction runs left to right. The + and − signs are the values of spins on the dual lattice. Figure taken from [1].

We can use equation (2.1.10) to define the Boltzmann weight $\rho[k]$ of a particular configuration $\{k\}$ of dimers as the product over the weights of each individual lattice

site.

$$\rho[k] = \prod_x w(k,x) \tag{2.1.11}$$

where $w(k,x)$ is the weight of site x in the configuration $\{k\}$ of dimers and

$$w(k,x) = \begin{cases} \phi(x) & \text{if } x \text{ contains a monomer} \\ 1 & \text{if 2 dimers at } x \text{ separated by } \pi \\ 1/\sqrt{2} & \text{if 2 dimers at } x \text{ separated by } \pi/2 \\ 0 & \text{otherwise.} \end{cases} \tag{2.1.12}$$

So far we have not taken homotopy classes into consideration. We define four partition functions–one for each homotopy class–by summing over all possible configurations of dimers within each class:

$$Z_k^{ij}[\phi] = \sum_{\{k(x,\mu)\} \in \mathcal{L}_{ij}} \rho[k] \tag{2.1.13}$$

where $i,j \in \{0,1\}$ indicate whether there exists a nontrivial loop winding in each direction. From equation (2.1.10) we see that the weight of a loop is positive for all configurations in $\mathcal{L}_{00}$.

The following connections between the dimer partition functions and the fermion partition functions hold, which are described in greater detail in [1]:

$$\begin{aligned} 4Z_k^{00}[\phi] &= +Z_\xi^{00}[\phi] + Z_\xi^{10}[\phi] + Z_\xi^{01}[\phi] + Z_\xi^{11}[\phi] \\ 4Z_k^{10}[\phi] &= -Z_\xi^{00}[\phi] + Z_\xi^{10}[\phi] - Z_\xi^{01}[\phi] + Z_\xi^{11}[\phi] \\ 4Z_k^{01}[\phi] &= -Z_\xi^{00}[\phi] - Z_\xi^{10}[\phi] + Z_\xi^{01}[\phi] + Z_\xi^{11}[\phi] \\ 4Z_k^{11}[\phi] &= -Z_\xi^{00}[\phi] + Z_\xi^{10}[\phi] + Z_\xi^{01}[\phi] - Z_\xi^{11}[\phi]. \end{aligned} \tag{2.1.14}$$

These relationships can be inverted to obtain partition functions for the fermions with definite boundary conditions in terms of the different classes of dimer partition functions. For example, the partition function for fermions with antiperiodic boundary

conditions in time and periodic boundary conditions in space is

$$Z_{\xi}^{10}[\phi] = +Z_{k}^{00}[\phi] + Z_{k}^{10}[\phi] - Z_{k}^{01}[\phi] + Z_{k}^{11}[\phi]. \tag{2.1.15}$$

The negative sign in front of $Z_{k}^{01}[\phi]$ means we have to sum contributions of negative weights and effectively amounts to the subtraction of statistics.

2.2 Wolff's Spin Representation

Here we sketch out the transformation of the dimer representation into a representation of lattices of Ising spins. This is the crucial aspect for the development of a Swendsen and Wang style cluster algorithm. The general idea is to conceive the dimer loops as boundaries of domains of up and down Ising spins which lie on the dual lattice. We can make this mathematically concrete by putting a field $s(\underline{x})$ of spins on the dual lattice and writing

$$k(x,\mu) = \begin{cases} 1 & \text{if } s(\underline{x})s(\underline{x}+\underline{\hat{\mu}}) = -1 \\ 0 & \text{if } s(\underline{x})s(\underline{x}+\underline{\hat{\mu}}) = +1 \end{cases} \tag{2.2.1}$$

where $\{\underline{x}\}$ are the sites of the dual lattice, located at the centers of the plaquettes of the original lattice, $s(\underline{x})$ is the value of the spin at $\underline{x}$, and $\underline{\hat{\mu}}$ is a unit vector on the dual lattice. A link on the original lattice $(x,\hat{\mu})$ is dual to the link $(\underline{x},\underline{\hat{\mu}})$ which crosses it. So if two adjacent spins are of the opposite sign, there is a dimer lying between them on the corresponding link of the original lattice; otherwise the spins are not separated by a dimer. An example of this is shown in Figure 2-3.

For each configuration of dimers, there are two possible configurations of spins on the dual lattice which obey equation (2.2.1). These two configurations differ simply by a global spin flip because, when populating the dual lattice with spins, there is a freedom in choosing the sign of the first spin. Examples of spins lying on the dual lattice can be seen in Figure 2-2.

The Boltzmann weight of a particular configuration of spins is a product over

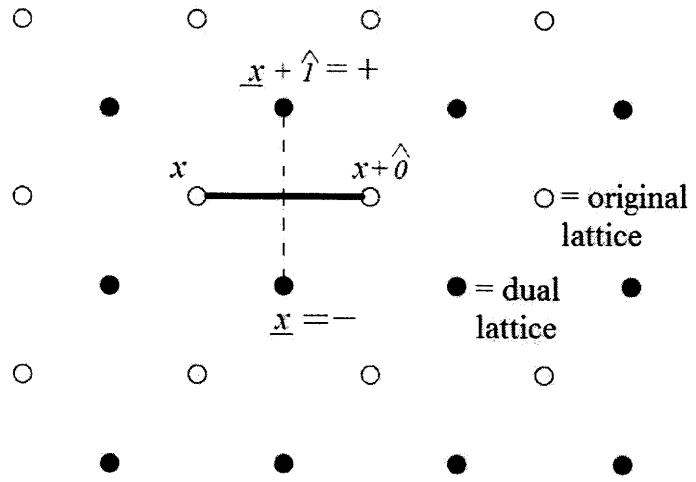

Figure 2-3: Diagram of the relationship between coordinates on the original lattice and dual lattice. A link exists on the original lattice between spins of opposite signs on the dual lattice. Figure taken and modified from [1].

all the plaquettes of the dual lattice, with a contribution $w(s_1, s_2, s_3, s_4)$ from each plaquette. If we label the spins around a plaquette as

$$\begin{pmatrix} s_4 & s_3 \\ s_1 & s_2 \end{pmatrix},$$

then we see that out of the 16 possible spin configurations, 2 are not allowed.

$$\begin{pmatrix} + & - \\ - & + \end{pmatrix} \quad \text{and} \quad \begin{pmatrix} - & + \\ + & - \end{pmatrix}$$

cannot exist because these correspond to intersecting loops on the original lattice. Therefore, though the spin fields $s(\underline{x})$ are composed of Ising-type spins, the set of allowed configurations is not equivalent to that of the Ising model.

We can define the weight of a plaquette on the spin lattice in terms of the relative signs of adjacent spins around the plaquette and unknown coefficients p, q, and r as

$$w(s_1, s_2, s_3, s_4) = p[\delta_{12}+\delta_{23}+\delta_{34}+\delta_{41}]+q[\delta_{12}\delta_{34}+\delta_{14}\delta_{23}]+r[\delta_{12}\delta_{14}+\delta_{21}\delta_{23}+\delta_{32}\delta_{34}+\delta_{41}\delta_{43}] \tag{2.2.2}$$

where $\delta_{ij} = \frac{1}{2}(1 + s_i s_j)$ are bonds. Since the plaquettes on the dual lattice correspond to the lattice points on the original lattice of dimers, we need the weights of the plaquettes on the spin lattice to match the weights of the lattice sites in the dimer representation. By evaluating the delta functions for the different possible configurations of spins around a plaquette (as shown in Table 2.1), we find that

$$\begin{aligned} \phi(x) &= 4p + 2q + 4r \\ \tfrac{1}{\sqrt{2}} &= 2p + r \\ 1 &= 2p + q. \end{aligned} \tag{2.2.3}$$

Solving for p, q, and r, we obtain the dependence of these coefficients on the mass parameter:

$$\begin{aligned} r &= \tfrac{1}{4}(\phi - 2) = \tfrac{m}{4} \\ p &= \tfrac{1}{2\sqrt{2}} - \tfrac{r}{2} \\ q &= 1 - \tfrac{1}{\sqrt{2}} + r. \end{aligned} \tag{2.2.4}$$

s_1	s_2	s_3	s_4	$w(s_1, s_2, s_3, s_4)$
$+(-)$	$+(-)$	$+(-)$	$+(-)$	$4p + 2q + 4r = \phi(x)$
$+(-)$	$+(-)$	$+(-)$	$-(+)$	$2p + r = \frac{1}{\sqrt{2}}$
$+(-)$	$+(-)$	$-(+)$	$+(-)$	$2p + r = \frac{1}{\sqrt{2}}$
$+(-)$	$-(+)$	$+(-)$	$+(-)$	$2p + r = \frac{1}{\sqrt{2}}$
$-(+)$	$+(-)$	$+(-)$	$+(-)$	$2p + r = \frac{1}{\sqrt{2}}$
$+(-)$	$-(+)$	$-(+)$	$+(-)$	$2p + q = 1$
$+(-)$	$+(-)$	$-(+)$	$-(+)$	$2p + q = 1$
$+(-)$	$-(+)$	$+(-)$	$-(+)$	0

Table 2.1: Weights of the 16 possible configurations of spins around a plaquette, where we have used the fact that $w(s_1, s_2, s_3, s_4) = w(-s_1, -s_2, -s_3, -s_4)$.

We can now define four spin partition functions in definite boundary conditions as

$$Z_s^\epsilon = \sum_{\{s(\underline{x})\}} \prod_{plaq} w(s_1, s_2, s_3, s_4) \tag{2.2.5}$$

where ϵ is the boundary condition for spins on the dual lattice. In order to relate these spin partition functions to the dimer partition functions, Z_k^ϵ, we must realize

that a nontrivial loop configuration in the k-representation in one direction forces antiperiodic spin boundary conditions in the s-representation in the corresponding orthogonal direction. This means that the following relationships between partition functions hold

$$Z_k^{00} = \frac{1}{2} Z_s^{00}, \quad Z_k^{10} = \frac{1}{2} Z_s^{01}, \quad Z_k^{01} = \frac{1}{2} Z_s^{10}, \quad Z_k^{11} = \frac{1}{2} Z_s^{11} \tag{2.2.6}$$

where the $\frac{1}{2}$ enters due to global spin flip symmetry. Note that for boundary conditions $\epsilon = (0,1)$ and $\epsilon = (1,0)$, the antiperiodic direction is opposite in Z_k and Z_s.

2.3 Negative Mass

The three coefficients of equation (2.2.4) are positive for masses such that $0 \leq m \leq 2\sqrt{2}$. This is sufficient for the free theory since, in this case, $m_c = 0$. However, for the theory of interacting fermions, it is necessary to allow for negative mass since $m_c < 0$ due to additive renormalization. The current bond probabilities p, q, r given in equation (2.2.4) restrict the algorithm we will use to $m \geq 0$ since otherwise $r < 0$ for negative m. In the negative mass case, we will need to use a new decomposition of the plaquette interaction by replacing the r term with

$$\frac{\tilde{r}}{2}[\delta_{12}\bar{\delta}_{14} + \delta_{21}\bar{\delta}_{23} + \delta_{32}\bar{\delta}_{34} + \delta_{41}\bar{\delta}_{43} + \bar{\delta}_{12}\delta_{14} + \bar{\delta}_{21}\delta_{23} + \bar{\delta}_{32}\delta_{34} + \bar{\delta}_{41}\delta_{43}] \tag{2.3.1}$$

where $\bar{\delta}_{ij} \equiv 1 - \delta_{ij}$ are antibonds, and keeping the other two terms the same, but making the substitutions $p \to \tilde{p}$ and $q \to \tilde{q}$. Setting the new weight and the old weight equal, we get the relations

$$\begin{aligned} \tilde{r} &= -r \\ \tilde{r} + \tilde{p} &= p \\ \tilde{q} &= q \end{aligned} \tag{2.3.2}$$

and plugging in the results of equation (2.2.4), we get the solution

$$\begin{aligned} \tilde{r} &= -\tfrac{1}{4}(\phi - 2) = \tfrac{-m}{4} \\ \tilde{p} &= \tfrac{1}{2\sqrt{2}} - \tfrac{\tilde{r}}{2} \\ \tilde{q} &= 1 - \tfrac{1}{\sqrt{2}} - \tilde{r}. \end{aligned} \tag{2.3.3}$$

We will need to use these alternate values when doing simulations with negative bare masses. The decomposition of equation (2.3.1) includes antibonds, which connect spins of opposite signs. This means that when using the cluster algorithm of the next chapter, if $m < 0$, clusters formed from these antibonds can include spins of both signs.

Chapter 3

A Cluster Algorithm for Simulating Free Fermions

We have seen that free fermions in $1+1$ dimensions can be represented as a system of Ising spins on a two dimensional latice. In order to calculate physical observables, we need a method to efficiently generate random lattice configurations. Since these fermions can be represented as Ising spins, we expect that it is possible to develop a method similar to the cluster algorithms for the Ising model of [3] and [4]. Cluster algorithms are much more efficient than local update algorithms. Here we develop a cluster algorithm for simulating free fermions in the spin representation. This algorithm constructs clusters of spins in order to generate independent spin configurations by using two Monte Carlo sampling techniques. In § 3.1, we describe the algorithm for simulating N flavors of free fermions on a lattice with definite spin boundary conditions. In § 3.2 we discuss the calculation of exact monomer densities for free fermions, and in § 3.3 we compare these exact calculations with free fermion simulations using the cluster algorithm of § 3.1.

3.1 Description of the Algorithm

We would like to sample configurations of spins from the partition function Z_s^ϵ, for a fixed value of ϵ. We will update spin configurations by constructing clusters of spins

and flipping the value of the spins in these clusters with some probability. As a first step, we will rewrite the weight of a single plaquette as

$$w(s_1, s_2, s_3, s_4) = \sum_{i=1}^{10} P_i \Delta_i(s_1, s_2, s_3, s_4) \tag{3.1.1}$$

where $P_i \in \{p, q, r\}$ and the Δ_i are the 10 delta function terms in equation (2.2.2). These Δ_i can be conceived as configuratons of bonds which lie on the links of the lattice of Ising spins. If $\delta_{ij} = 1$, there is a bond between s_i and s_j, otherwise, there is no bond.

In order to construct clusters of spins, we will first sample the Δ_is. To do this, we will restructure the partition function as follows. Introduce bond variables $b(x)$ which take on the values $\{1, ..., 10\}$ and represent the 10 possible configurations of bonds around a single plaquette (see Table 3.1). Sum over all possible configurations of these bond variables on the original lattice in addition to all possible configurations spins on the dual lattice to get

$$Z_s = \sum_{\{b(x), s(\underline{x})\}} \prod_{\text{plaq}} P_{b(x)} \Delta_{b(x)}(s_1, s_2, s_3, s_4). \tag{3.1.2}$$

With the partition function now written this way, we can sample both the bond variables and the spins. These three steps are required to generate one new spin

$b(x)$	$P_{b(x)}$	$\Delta_{b(x)}$
1	p	δ_{12}
2	p	δ_{23}
3	p	δ_{34}
4	p	δ_{41}
5	q	$\delta_{12}\delta_{34}$
6	q	$\delta_{14}\delta_{23}$
7	r	$\delta_{12}\delta_{14}$
8	r	$\delta_{21}\delta_{23}$
9	r	$\delta_{32}\delta_{34}$
10	r	$\delta_{41}\delta_{43}$

Table 3.1: Values of bond probabilities P_i and Δ_i for bond variables $b(x)$.

configuration.

1. Choose a new configuration of bond variables, $\{b(x)\}$, at fixed spins by a local heatbath procedure. That is, sweep through the lattice and at each site x, choose a new $b(x) \in \{1, ..., 10\}$ with probability

$$p(b(x)) = \frac{P_{b(x)}\Delta_{b(x)}(s_1, s_2, s_3, s_4)}{\sum_{i=1}^{10} P_i \Delta_i(s_1, s_2, s_3, s_4)}. \tag{3.1.3}$$

   Note that some values for $b(x)$ may have zero probability because $\Delta_i(s_1, s_2, s_3, s_4) = 0$ for some i and some configurations of four spins. For example, for $s_1 = s_2 = s_3 = +$ and $s_4 = -$, the only possible values for $b(x)$ with nonzero probability are $b(x) = 1, 2$, or 8 because Δ_1, Δ_2, and Δ_8 are the only nonzero delta function terms.

2. Construct clusters of spins based on this new bond configuration. The set of bond variables $\{b(x)\}$ maps out a configuration of bonds lying on links between spins. This bond configuration completely specifies the set of clusters. Two spins which are joined by a bond belong to the same cluster.

3. For each cluster, either flip all of the spins in the cluster or flip none of them. Choose each option with probability 1/2. This results in the selection of one of the possible equally weighted configurations of spins.

Performing these steps constitutes one iteration of the algorithm, after which we have sampled one new configuration of spins.

Simulating multiple flavors of fermions is trivial in the case of the free theory. Each flavor is represented by an Ising lattice of spins, meaning that for N flavors, there are N spin values at each lattice point. Each of the N lattices is updated independently according to the steps described above, and the update procedure for one lattice is not affected by the values of the spins in the other $N-1$ lattices. This will no longer be true in the interacting theroy, and we will return to this discussion in Chapter

4. After each lattice has been updated, we have sampled one new configuration of $(Z_s^{\epsilon}[\phi])^N$.

If we want to sample configurations of the spin partition function with boundary conditions other than $\epsilon = (0,0)$, we have to modify the algorithm such that spins which lie on an edge with antiperiodic boundary conditions see each other as the opposite sign. This only affects the weights of plaquettes along an antiperiodic edge, which should be adjusted for when computing bond probabilities.

3.2 Exact Monomer Densities for Free Fermions

To test the effectiveness of our algorithm, we would like to compute an observable which can be calculated exactly. One such observable we can calculate is the average monomer density $\langle K \rangle$. $K(x) = 1$ if there is a monomer at x and 0 otherwise. In the spin representation, this is just

$$K(x) = \delta_{|s_1+s_2+s_3+s_4|,4} \tag{3.2.1}$$

which evaluates to 1 only if the four spins around x are the same. $\langle K \rangle$ can be computed exactly for free fermions in any combination of boundary conditions using the methods described in [1]. In the free theory $\langle K \rangle$ is directly proportional to the more interesting observable, the fermion condensate $\langle \bar{\psi}\psi \rangle$, or $\langle \xi^{\top} C \xi \rangle$ in terms of Majorana fermions, as

$$\langle K \rangle = -\frac{\phi}{2} \langle \xi^{\top} C \xi \rangle \tag{3.2.2}$$

where $\phi = 2 + m$. Monomer densities ar a good starting point to verify the algorithm because they are easy to compute exactly and because, as we move to the interacting theory, we will want to compute $\langle \xi^{\top} C \xi \rangle$. In the next section, we discuss calculations of $\langle K \rangle$ in fermion simulations.

Boundary Conditions	Lattice Size	$\langle K \rangle$	τ_{int}	Exact Value
$\epsilon = (0,0)$	8×8	0.80733(32)	1.58(2)	0.80738
	16×16	0.78882(21)	1.92(2)	0.78914
	32×32	0.77950(13)	2.36(3)	0.77951
$\epsilon = (0,1)$	8×8	0.66989(26)	1.75(2)	0.66966
	16×16	0.71786(15)	1.61(2)	0.71808
	32×32	0.74367(9)	1.81(2)	0.74378
$\epsilon = (1,1)$	8×8	0.61263(18)	1.38(1)	0.61277
	16×16	0.69264(12)	1.39(1)	0.69272
	32×32	0.73151(8)	1.59(2)	0.73146

Table 3.2: The monomer density and integrated autocorrelation time computed for three square lattice sizes and three boundary conditions using the cluster algorithm. The results are very close to the exact values.

3.3 Simulations of Free Fermions

$\langle K \rangle$ was computed using the cluster algorithm for three different lattice sizes and in three different boundary conditions ($\epsilon = (1,0)$ is equivalent to $\epsilon = (0,1)$ on a square lattice). The results of these simulations are shown in Table 3.2. The exact values are within errors of the results. Each run had 6×10^5 iterations, with a small fraction discarded to allow for equilibration. The integrated autocorrelation time τ_{int} measures the average number of iterations over which configurations are correlated and is given by

$$\tau_{int} = \frac{1}{2} + \sum_{t=1}^{N-1} \frac{\Gamma(t)}{\Gamma(0)} \tag{3.3.1}$$

where

$$\Gamma(t) = \langle a_i a_{i+t} \rangle - \langle a_i \rangle \langle a_{i+t} \rangle \tag{3.3.2}$$

is the connected correlation of measurements a_i that are t computer time steps apart, and $\Gamma(0)$ is just the variance of the measurements. With this definition of τ_{int}, the error σ on the measurement is given by

$$\sigma^2 = \frac{2\tau_{int}}{N}\Gamma(0). \tag{3.3.3}$$

Values for $\langle K \rangle$, errors, and τ_{int} were computed using the methods described in [9]. Both $\langle K \rangle$ and τ_{int} are consistent with the results obtained by Wolff in [1]. The run time scaled approximately as the order of the size of the lattice. Everything was computed on the order of minutes using a laptop.

In general, the autocorrelation time slightly increases with increasing lattice size. This algorithm is *much* more efficient than local algorithms, which have autocorrelations which scale with the lattice volume [1]. In addition, errors on the value of $\langle K \rangle$ decrease with increasing lattice size roughly as $1/TL$, adjusted by the slightly increasing autocorrelation time. τ_{int} is lower for simulations with increasingly antiperiodic boundary conditions, as found in [1].

Chapter 4

Simulations of Interacting Fermions

Now that it is possible to simulate free fermions on a two dimensional lattice using a cluster algorithm with efficiency much greater than that of known local updating algorithms, it would be much more interesting to apply this technique to the interacting theory, where correlation functions cannot be calculated exactly. In this chapter, we discuss the application of the cluster algorithm of Chapter 3 to the Gross-Neveu model. In § 4.1, we describe how to modify the algorithm to simulate N flavors of interacting fermions. § 4.2 discusses how to calculate fermion correlation functions using this algorithm. We present the first results of simulations of the Gross-Neveu model using a cluster algorithm in § 4.3 (for doubly periodic spin boundary conditions) and in § 4.4 (for singly and doubly antiperiodic boundary conditions).

4.1 Modification of the Cluster Algorithm

The algorithm described in § 3.1 must be modified in order to simulate N flavors of interacting fermions. To model N flavors of interacting fermions, we will use N Ising lattices (one for each fermion). This means that at each site there are N spins (one from each lattice.) The total weight of a particular configuration is a product over the weights of the plaquettes of each of the N lattices. The weights of plaquettes that

do not contain monomers are numerical constants and so are unchanged. However, the monomer weights are modified due to the interactions between fermions. $w(x) = \phi(x) = 2 + m(x)$ is replaced by an effective monomer weight $\phi_{\bar{n}}(x)$ which depends on the total number of monomers at site x and the value of the coupling, g. The inclusion of these effective monomer weights is the only difference between the algorithm for the free theory and the algorithm for the Gross-Neveu model [1].

We can calculate these effective monomer weights using equation (1.2.9). If there are n monomers at site x, then the weight of site x comes from the interactions of all the monomers at x and is given by

$$c(n, m, g) = \exp\left\{\frac{g^2}{2}\frac{\partial^2}{\partial m^2}\right\}(2+m)^n = \sum_{j=0}^{\lfloor n/2 \rfloor} \frac{n!}{2^j j!(n-2j)!} g^{2j}(2+m)^{n-2j}. \quad (4.1.1)$$

This means that we can replace $\phi(x)$ with the effective monomer weight

$$\phi_{\bar{n}}(x) = \frac{c(\bar{n}(x)+1, m, g)}{c(\bar{n}(x), m, g)} \quad (4.1.2)$$

where $\bar{n}(x)$ = number of monomers at site x in the $N-1$ lattices not currently being updated. The first few effective monomer weight values are

$$\phi_0(x) = 2 + m; \quad \phi_1(x) = 2 + m + \frac{g^2}{2+m}; \quad \phi_2(x) = 2 + m + \frac{2g^2(2+m)}{(2+m)^2 + g^2} \quad (4.1.3)$$

In one iteration of the algorithm, each spin lattice is updated independently. The effective mass only enters the update routine in the step where the bond variables are updated through the coefficients p, q, and r, which depend on the value of ϕ.

4.2 Calculation of Correlation Functions

We would like to use our algorithm to generate most probable configurations of the Gross-Neveu partition function in order to calculate fermion correlation functions. We can test the correctness of our algorithm by computing these observables and comparing them to exact results at $g = 0$, and to results calculated by other methods

for $g \neq 0$. Here we will derive equations for correlation functions in the spin representation. The observables we will discuss are the chiral condensate and the mass susceptibility, which can be written as derivatives of the partition function.

Define χ, the chiral condensate, as

$$\chi = \langle \xi^\top C \xi \rangle = -\frac{1}{V} \frac{\partial \ln Z_s^\epsilon}{\partial m} \tag{4.2.1}$$

where $V = TL$ is the total number of lattice sites. The spin partition function from equation (2.2.5) can be written as

$$Z_s^\epsilon = \int ds \prod_x w(x) \tag{4.2.2}$$

where $\int ds$ indicates a summation over all possible spin configurations and $w(x)$ is the weight of the plaquette at x, taking into account the effective monomer weights from equation (4.1.2). Plugging equation (4.2.2) into equation (4.2.1), we get

$$\chi = -\frac{1}{V}\frac{1}{Z}\frac{\partial Z}{\partial m} = -\frac{1}{V}\frac{1}{Z}\int ds \sum_x \left(\prod_{x' \neq x} w(x') \right) \frac{\partial w(x)}{\partial m}. \tag{4.2.3}$$

We can rearrange this by multiplying and dividing the integrand by $w(x)$ to give

$$\chi = -\frac{1}{V}\frac{1}{Z}\int ds \left(\sum_x \frac{1}{w(x)} \frac{\partial w(x)}{\partial m} \right) \prod_x w(x). \tag{4.2.4}$$

The equation is now in the form $\chi = -\frac{1}{V}\frac{1}{Z}\int ds \hat{O} \prod_x w(x)$, so we must sample the operator

$$\hat{O} = \sum_x \frac{1}{w(x)} \frac{\partial w(x)}{\partial m} \tag{4.2.5}$$

for each spin configuration and average over these independently generated measurements of $\hat{O}$ to compute a value for χ.

The mass susceptibility C_χ is a measure of how the chiral condensate changes with an infinitesimal change in the mass parameter and can be written as the second

derivative of the partition function

$$C_\chi = \frac{\partial \chi}{\partial m} = -\frac{1}{V}\frac{\partial^2 \ln Z}{\partial m^2}. \tag{4.2.6}$$

Following the same steps we used to compute the equation for χ in the spin representation, we get

$$\begin{aligned} C_\chi &= \frac{\partial}{\partial m}\left[-\frac{1}{V}\frac{1}{Z}\int ds \left(\sum_x \frac{1}{w(x)}\frac{\partial w(x)}{\partial m}\right)\prod_x w(x)\right] \\ &= V\chi^2 - \frac{1}{V}\frac{1}{Z}\int ds \prod_x w(x)\left(\sum_x \frac{1}{w(x)}\frac{\partial w(x)}{\partial m}\right)^2 \\ &\quad - \frac{1}{V}\frac{1}{Z}\int ds \prod_x w(x)\sum_x\left(\frac{1}{w(x)}\frac{\partial^2 w(x)}{\partial m^2} - \frac{1}{w(x)^2}\left(\frac{\partial w(x)}{\partial m}\right)^2\right). \end{aligned} \tag{4.2.7}$$

Therefore, in order to compute C_χ we have to sample the operator

$$\left(\sum_x \frac{1}{w(x)}\frac{\partial w(x)}{\partial m}\right)^2 + \sum_x\left(\frac{1}{w(x)}\frac{\partial^2 w(x)}{\partial m^2} - \frac{1}{w(x)^2}\left(\frac{\partial w(x)}{\partial m}\right)^2\right) \tag{4.2.8}$$

in each spin configuration and also use our calculated result for χ. The derivatives of $w(x)$ which appear in equations (4.2.5) and (4.2.8) are only nonzero if there is a monomer at x and can be computed by taking derivatives of equation (4.1.2). Calculations of χ and C_χ for the Gross-Neveu model are discussed in the next two sections.

4.3 Results for the Gross-Neveu Model

The results presented in this section were all computed with $\epsilon = (0, 0)$ spin boundary conditions with all spins pointing in the same direction as an initial condition. We begin with further results for the free case. The chiral condensate was calculated as a function of the mass parameter m using the cluster algorithm of § 4.1 and the prescription of § 4.2 for two free Majorana fermions for 8×8 and 16×16 square

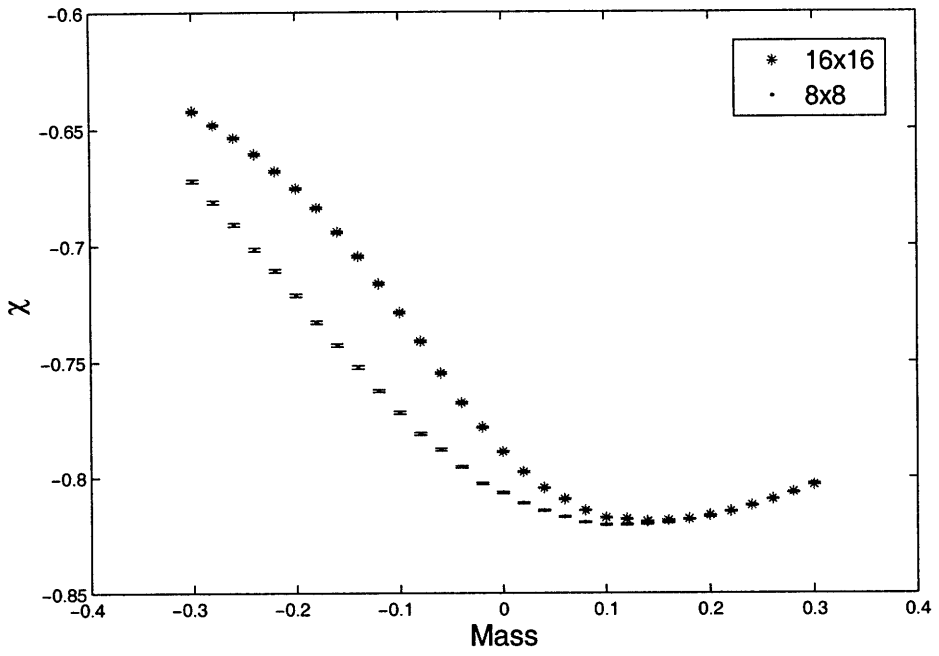

Figure 4-1: Chiral condensate of two free Majorana fermions ($g^2 = 0$) as a function of the mass parameter computed for two square lattice sizes.

lattices and is shown in Figure 4-1. Similarly, the mass susceptibility was computed as a function of m for two free Majorana fermions and is shown in Figure 4-2. We used $O(10^4)$ measurements of observables per data point, and could produce one curve in on the order of an hour using a laptop. The statistical errors for all of the measurements in this section were computed from integrated autocorrelation times using the methods of [9]. We see a peak in the magnitude of the susceptibility that moves to the right as the lattice size increases. This peak diverges logarithmically with L^2 at $m = 0$, as calculated in [10] and [11] for lattice sizes up to 512^2 and 700^2.

Similar plots were produced of χ and C_χ for one Dirac fermion using a loop algorithm in [11]. The results we obtain for two Majorana fermions are quantitatively equivalent to the results obtained for one Dirac fermion, as expected. Therefore, we reconfirm that the cluster algorithm is working properly for the the free theory, and we conclude that our methods for computing χ and C_χ in the spin representation are correct. Though these results were obtained on the order of minutes using a

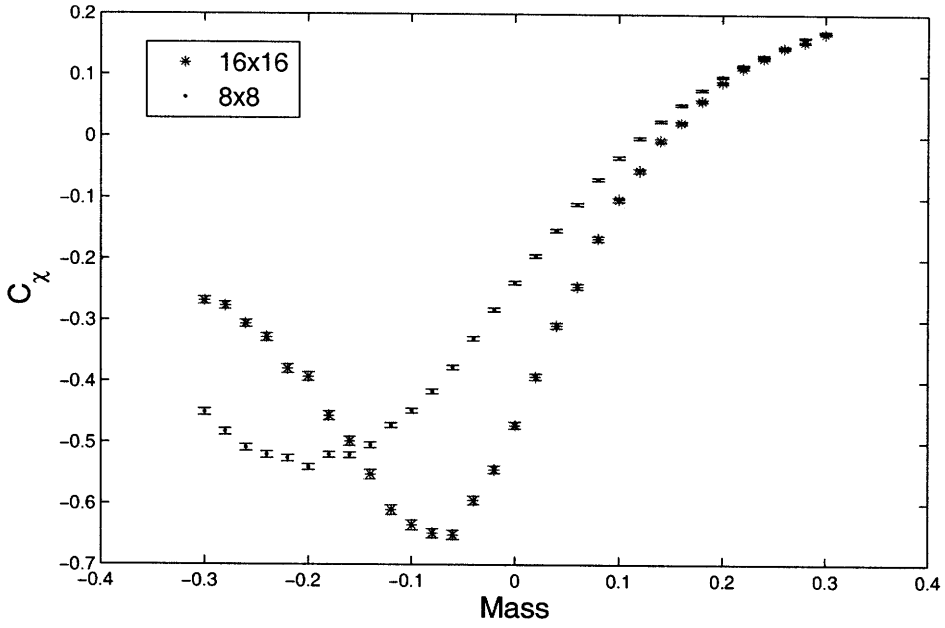

Figure 4-2: Mass susceptibility of two free Majorana fermions ($g^2 = 0$) as a function of the mass parameter computed for two square lattice sizes.

laptop, and it is well within our capability to extend these calculations to larger lattice sizes, we do not feel the need to do so, as we expect to obtain results which are quantitatively equivalent to those presented in [11]. For the two lattice sizes we did explore, we observe that for $m \gtrsim 0.2$, the values of χ and C_χ no longer differ. The differences at $m \lesssim 0.2$ are due to effects from the finite size of the lattice.

For the interacting theory, plots of the condensate and mass susceptibility for two Majorana fermions at coupling $g^2 = 0.1$ are shown in Figure 4-3 and Figure 4-4 respectively. The shapes of the curves in the interacting case are qualitatively similar to those of the free theory, but the correlation functions take on different values due to the nonzero fermion coupling. These plots can once again be compared with plots obtained using a loop algorithm for one Dirac fermion in [11]. We find that the curves of χ and C_χ are equivalent to those in [11], and thus conclude that our algorithm works properly for the theory of interacting Gross-Neveu fermions. The peaks in the susceptibility are shifted to the left from their location in the free theory ($g^2 = 0$). If we assume that calculations for larger lattices will be the same as those

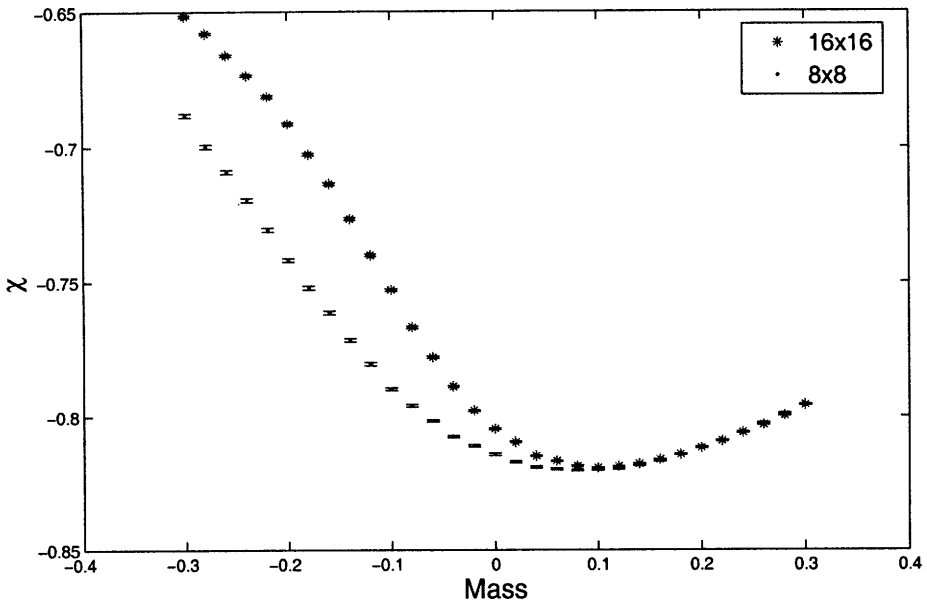

Figure 4-3: Chiral condensate of two interacting Majorana fermions ($g^2 = 0.1$) as a function of the mass parameter computed for two square lattice sizes.

obtained in [11], we expect that the critical mass is no longer at $m = 0$, but occurs at a negative value of the mass parameter. Again, we see the disappearance of finite size effects at high values of the mass parameter. Though we have not computed correlation functions for lattice sizes greater than 16×16, we expect that finite size effects will also disappear with large lattice sizes at low values of the mass parameter and only remain manifest at the critical mass, as in [11].

These are the first results for the Gross-Neveu model using a cluster algorithm. The enormous improvement in efficiency over local algorithms make this algorithm an excellent tool to numerically study interacting fermions in $1 + 1$ dimensions. In the next chapter we will use this tool to investigate phase transitions of interacting fermions. But before we conclude this chapter, we will present results for the Gross-Neveu model in spin boundary conditions other than $\epsilon = (0, 0)$.

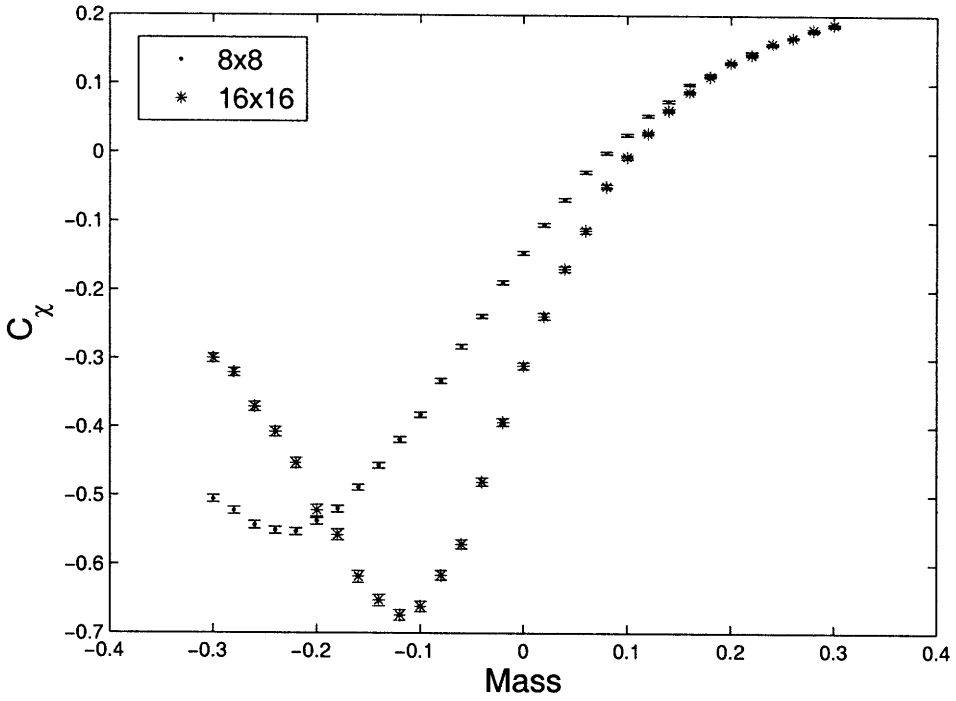

Figure 4-4: Mass susceptibility of two interacting Majorana fermions ($g^2 = 0.1$) as a function of the mass parameter computed for two square lattice sizes.

4.4 Boundary Conditions

Here we present results for interacting fermions in fixed spin boundary condtions $\epsilon = (0,1)$ and $\epsilon = (1,1)$. Figure 4-5 shows χ computed as a function of the mass parameter for a 32×32 lattice with $g^2 = 0$ for these three boundary conditions. Because $\epsilon = (1,0)$ boundary conditions are equivalent to $\epsilon = (0,1)$ on a square lattice, $\epsilon = (1,0)$ was omitted. We see finite size effects due to the different boundary conditions. At small values of m, there is no distinction in the value of the condensate for different boundary condtions, however, at large m a gap emerges. This agrees with the results obtained in [11]. As the boundary conditions become increasingly periodic, the magnitude of the condensate decreases for high values of m, as was found in [11]. This is due to the fact that for $\epsilon = (0,0)$, there are no nontrivial loops on the latice, and at high mas there are a greater number of monomers than in the boundary conditions $\epsilon = (0,1)$ and $\epsilon = (1,1)$. Figure 4-6 shows C_χ as a function of m on a

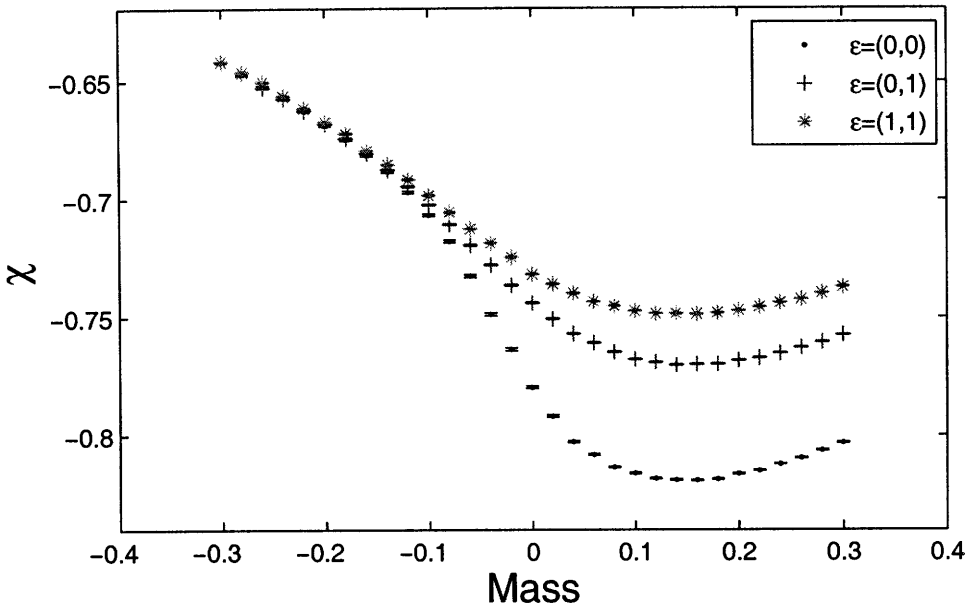

Figure 4-5: Chiral condensate as a function of the mass parameter for 2 Majorana fermions on a 32×32 lattice with $g^2 = 0$. $\epsilon = (0,0)$, $\epsilon = (0,1)$ and $\epsilon = (1,1)$ boundary conditions were used.

32×32 lattice with $g^2 = 0$ for the same three boundary conditions. We see that the cusp in the mass susceptibility is sharper for doubly periodic boundary conditions, $\epsilon = (0,0)$, indicating a steeper transition in the condensate at $m = 0$, as observed in Figure 4-5. At high and low values of m, there is no difference in C_χ between the different boundary conditions.

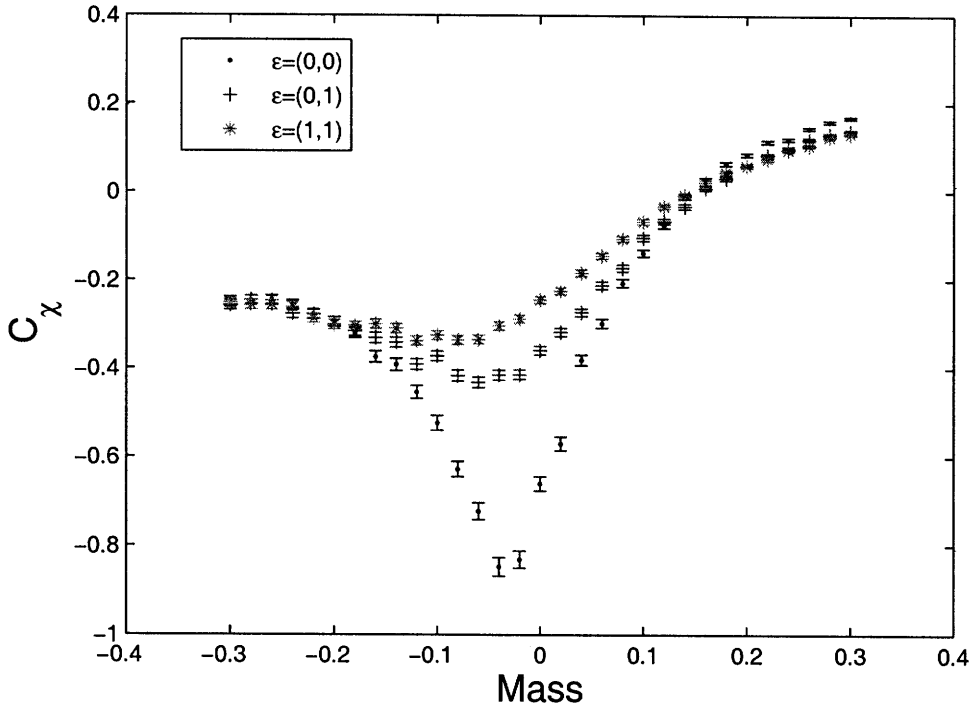

Figure 4-6: Mass susceptibility as a function of the mass parameter for 2 Majorana fermions on a 32×32 lattice with $g^2 = 0$. $\epsilon = (0, 0)$, $\epsilon = (0, 1)$ and $\epsilon = (1, 1)$ boundary conditions were used.

Chapter 5

Gross-Neveu Fermions at Nonzero Temperature

Now that we have developed an efficient cluster algorithm to accurately simulate Gross-Neveu model fermions, we can use this technique to further investigate the properties of interacting fermions in $1+1$ dimensions. We would like to observe the second order phase transition from spontaneously broken chiral symmetry to restored chiral symmetry which occurs at a nonzero critical temperature. We can analyze fermions at nonzero temperature by using boundary conditions which are antiperiodic in the time direction (this leads to the correct Fermi-Dirac distribution of particles.) From equation (2.1.15), we know that in order to simulate the fermion partition function with $\epsilon = (1,0)$, we have to simulate all four possible spin partition functions. Yet, this equation contains a negative contribution from the Z_k^{01} partition function, so when simulated, we would effectively be subtracting statistics from our calculation of observables, wasting computer time. If we reach the infinite spatial volume limit, however, the boundary conditions in the space direction should not matter. Therefore, to avoid simulating a negative partition function, and to make our algorithm slightly simpler, we will leave the boundary condition in the space direction variable and instead simulate

$$Z_\xi^{10} + Z_\xi^{11} = 2(Z_k^{10} + Z_k^{00}) = Z_s^{01} + Z_s^{00} \tag{5.0.1}$$

which can easily be derived from equation (2.1.14).

To simulate fermions at nonzero temperature, we need to sample spin configurations from two different classes of boundary conditions, $\epsilon = (0,0)$ and $\epsilon = (0,1)$, which are periodic in the time direction and either periodic or antiperiodic in the space direction. This reversal of boundary conditions comes from the correspondence of spin and loop partition functions described in equation (2.2.6). In § 5.1 we describe an algorithm for simulating the partition function combination of equation (5.0.1) using fluctuating boundary conditons. We test the accuracy of this algorithm by comparing simulations of free fermions to exact results for the free theory in § 5.2 and checking its self-consistency in the interacting theory in § 5.3. The results of the first simulations of Gross-Neveu fermions at nonzero temperature using a cluster algorithm are presented in § 5.4.

5.1 Fluctuating Boundary Conditions

Here we construct an algorithm for sampling spin configurations from the partition function $Z_{tot} = Z_s^{01} + Z_s^{00}$. Now each of the N spin lattices will have an associated boundary condition variable which is independent of the boundary conditions of the other lattices. At each iteration of the algorithm, first all of the spins are updated using the procedure described in §3.1. Then the program will attempt to update the boundary conditions of each lattice of spins. The idea of the algorithm is to look for some axis perpendicular to the space direction, which we will call a horizontal cut(assuming the time direction points horizontally and the space direction points vertically.) Then, with some probability, flip the spins above the cut while leaving the ones below fixed and, at the same time, change the spatial boundary conditions. We are only interested in changing the spatial boundary conditions, so our axis must be a nontrivial loop in the time direction. Though we could in principle search for any loop which begins and ends at the same plaquette point and winds around the lattice in the time direction to serve as our boundary for flipping spins, it is simpler and just as effective to only search for a horizontal line.

This combined process of flipping spins and changing boundary conditions will only affect the weights of the plaquettes along the cut (and therefore the probability of making this update will be proportional to the weights of the plaquettes along the cut in the old configuration and the proposed configuration). Not any horizontal axis can function as a cut, however, because in general illegal plaquettes may arise by flipping the spins on one side of the cut. The algorithm for finding a horizontal cut and updating the boundary conditions of a single spin lattice consists of the following steps:

1. Sweep through the lattice of bond variables and propose a new bond at each lattice site. Each of $b(x) = 1$ and $b(x) = 3$ are proposed with probability $1/2$. These bond types connect spins horizontally and thus will increase the probability of there being a horizontal cut through the lattice.

2. Accept the proposed bond value with probability

$$P_{accept} = \min\left(1, \frac{P_{b'(x)}\Delta_{b'(x)}(s_i)}{P_{b(x)}\Delta_{b(x)}(s_i)}\right) \tag{5.1.1}$$

   where $b(x)$ is the current bond value and $b'(x)$ is the proposed bond value.

3. Sweep through the lattice of bond variables and look for a horizontal cut. A horizontal cut exists if there is an entire row of the lattice with $b(x) \in 1, 3, 5$. Otherwise, there are vertical bonds across the horizontal axis and the axis cannot be used as a cut.

4. If there exists a cut, flip the spins above the cut with probability

$$P_{flip} = \frac{\prod_{x \text{ along cut}} w'(x)}{\prod_{x \text{ along cut}} w(x)} \tag{5.1.2}$$

   where $w'(x)$ is the weight at x in the proposed configuration with flipped spins and $w(x)$ is the weight at x in the current configuration.

5. If the spins were flipped, change the spatial boundary condition from periodic to antieriodic or vice versa. Otherwise do nothing.

This algorithm is repeated for each of the N lattices. Once the boundary conditions have been updated for each lattice a new configuration has been sampled. In the next section we will check the correctness of the algorithm for fluctuating boundary conditions by comparing calculations of correlation functions in the boundary conditions $Z_\xi^{10} + Z_\xi^{11}$ to exact results for the free theory. With both the fluctuating boundary conditions algorithm verified in the free case and the cluster algorithm at fixed boundary conditions verified for the interacting theory independently, we expect that the combination of the two will produce correct results for the interacting theory using fluctuating boundary conditions.

5.2 Exact Results for the Free Theory

We would first like to test that our algorithm of § 5.1 correctly simulates the partition function of equation (5.0.1). In this section we will compare results of free fermion simulations in the boundary conditions $Z_s^{00} + Z_s^{01} = Z_\xi^{10} + Z_\xi^{11}$ to exact values of correlation functions. The chiral condensate can be calculated exactly for N free Majorana fermions in any combination of fermion boundary conditions

$$\bar{Z}_\xi[m] = \sum_\epsilon c(\epsilon) Z_\xi^\epsilon[m] \tag{5.2.1}$$

and is given by

$$-\frac{1}{2}\langle \xi^\top C \xi \rangle_c = \frac{1}{TL}\frac{\partial}{\partial m} \ln(\bar{Z}_\xi). \tag{5.2.2}$$

This only depends on the parameters T, L, and m. A method for calculating equation (5.2.2) using exact fermion partition functions is described in [1].

First, we simulate one free Majorana fermion. In Figure 5-1, we show the results of calculations of χ as a function of the mass parameter for a lattice of size $T = 4, L = 16$ using the algorithm of § 5.1. Also plotted are the exact values of the condensate for $\bar{Z}_\xi = Z_\xi^{10} + Z_\xi^{11}$. The values obtained as a result of simulations are in agreement with

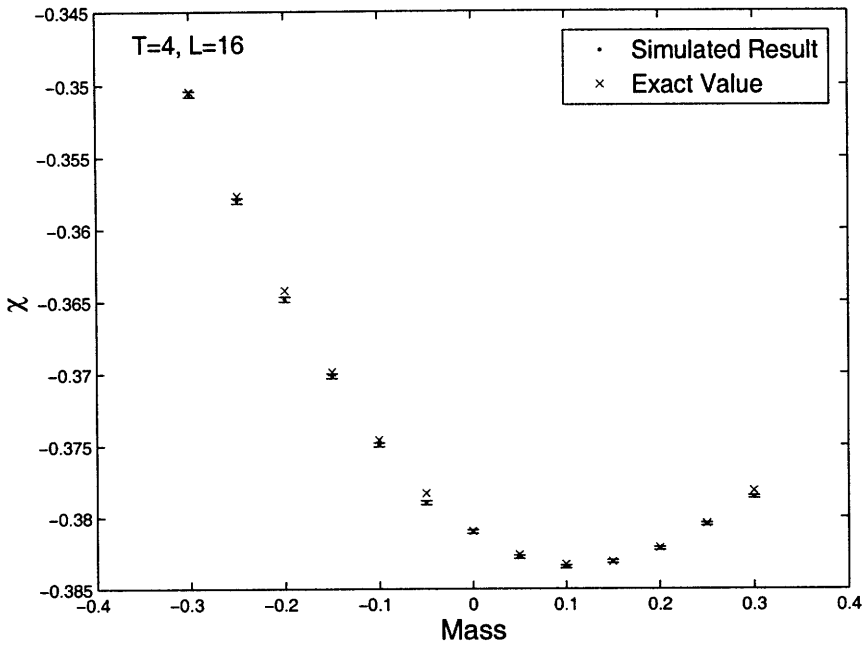

Figure 5-1: Exact and simulated chiral condensate of one free Majorana fermion as a function of the mass parameter on a rectangular lattice with $T = 4$ and $L = 16$. The boundary conditions of the simulation were sampled from the partition function $Z_s^{00} + Z_s^{01}$ using the algorithm of § 5.1.

the exact results, and thus we determine that the algorithm for fluctuating boundary conditions works correctly in the case of one free fermion. Figure 5-2 shows a similar plot for a lattice of size $T = 16, L = 4$, demonstrating the asymmetry of the time and space directions. The shape of the curve is slightly different when we change the orientation of the lattice due to the fluctuating boundary conditions in the spatial direction.

We obtain values of the condensate which match the exact results for multiple species of free fermions as well (in the case $\chi_{Nflavors} = N\chi_{1flavor}$). The consistency of the numerical values of χ with the exact values is similar to that seen in Figures 5-1 and 5-2 for one free fermion, but we do not find it illuminating to present plots of this here. From this, we conclude that the algorithm works properly for the free theory. In the next section we check the consistency of the algorithm in the case of the interacting theory.

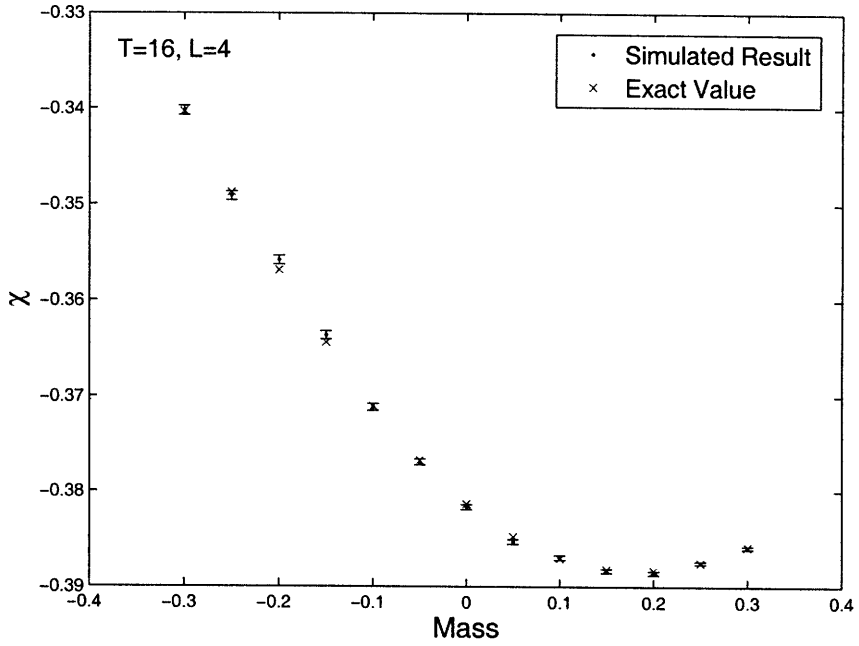

Figure 5-2: Exact and simulated chiral condensate of one free Majorana fermion as a function of the mass parameter on a rectangular lattice with $T = 16$ and $L = 4$. The boundary conditions of the simulation were sampled from the partition function $Z_s^{00} + Z_s^{01}$ using the algorithm of § 5.1.

5.3 Correlation Functions in the Interacting Theory

Here we consider multiple flavors of Gross-Neveu fermions with the boundary conditions of equation (5.0.1) using the algorithm outlined in § 5.1. Because we cannot exactly calculate observables in the interacting theory and because results for this model have not been obtained by any other methods previously, we cannot compare the calculations of correlation functions we obtain to any other values. Instead, we will check the self-consistency of the algorithm in the interacting theory before using it to study Gross-Neveu fermions at nonzero temperature.

To check the consistency of the algorithm for calculating correlation functions using fluctuating boundary conditions, we calculate the mass susceptibility in two ways and compare the results. We do simulations of two Majorana fermions on a

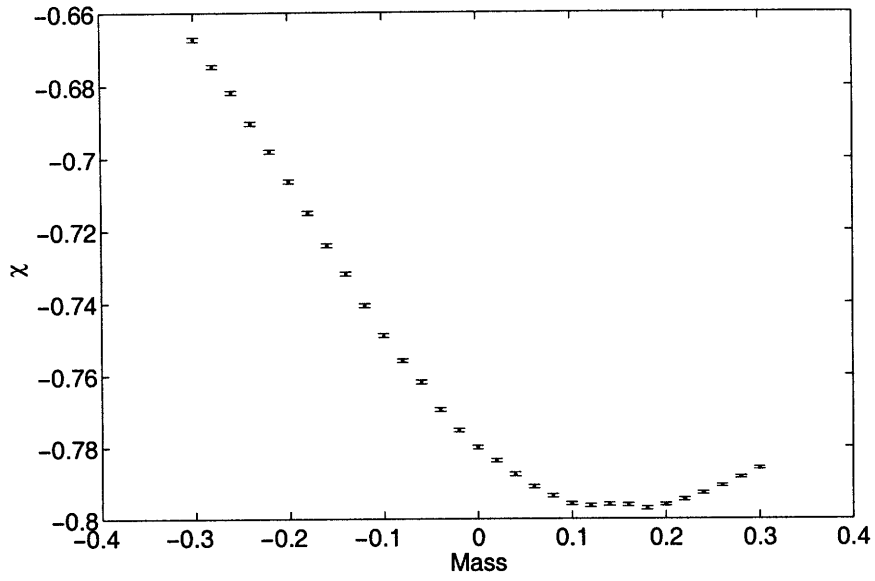

Figure 5-3: Chiral condensate of two interacting Majorana fermions ($g^2 = 0.1$) as a function of the mass parameter on an 8×8 lattice with fluctuating boundary conditions.

square 8×8 lattice with coupling $g^2 = 0.1$. Figure 5-3 and Figure 5-4 show calculations of the condensate and the mass susceptibility, respectively, as a function of the mass parameter done using the method of § 5.1 for fluctuating boundary conditions. Both were also computed previously using the prescription presented in § 4.2. The results in Figures 5-3 and 5-4 are qualitatively similar to those presented in § 4.3 but differ numerically because of the difference in boundary conditions.

We also approximate the mass susceptibility for two flavors of interacting ($g^2 = 0.1$) fermions on an 8×8 lattice by calculating the numerical derivative of the condensate. The numerical derivative is defined as

$$\tilde{C}_\chi(m) = \frac{\Delta\chi}{\Delta m} = \frac{\chi\left(m + \frac{\Delta m}{2}\right) - \chi\left(m - \frac{\Delta m}{2}\right)}{\Delta m}. \tag{5.3.1}$$

In Figure 5-5 we plot the numerical derivative $\tilde{C}_\chi$ calculated using $\Delta m = 0.08$ and the values for the condensate plotted in Figure 5-3. We also plot the calculations of C_χ directly from the simulations which are shown in Figure 5-4. We see that the two sets of results are well within errors of each other and that our method for computing

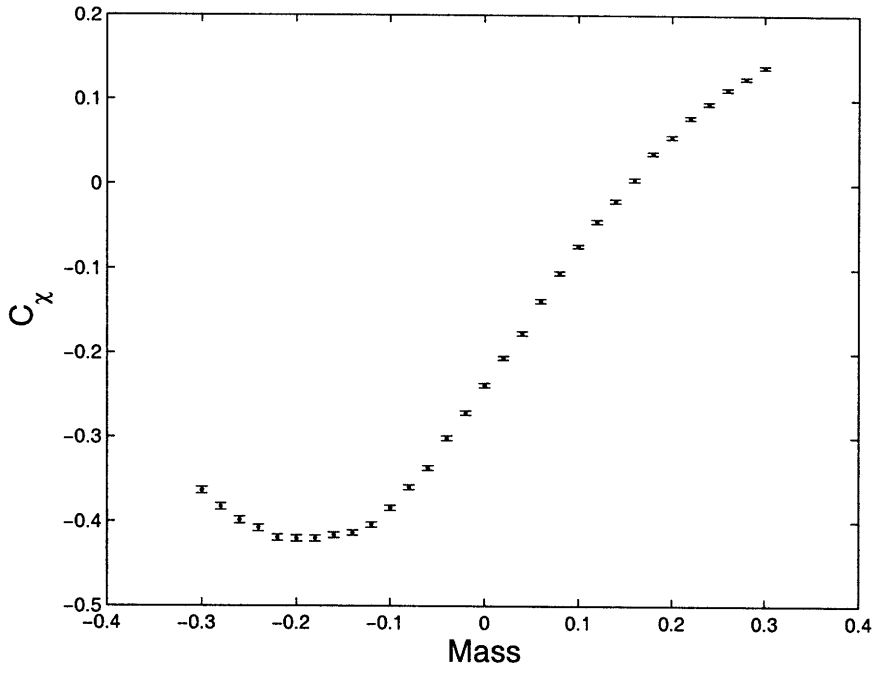

Figure 5-4: Mass susceptibility of two interacting Majorana fermions ($g^2 = 0.1$) as a function of the mass parameter on an 8×8 lattice with fluctuating boundary conditions.

correlation functions using this algorithm is self-consistent. Now we can confidently use this algorithm to study Gross-Neveu fermions at nonzero temperature.

5.4 Fermion Phase Transitions

We can simulate fermions at nonzero temperature by using a rectangular lattice which is very long in the spatial direction and short in the time direction. The number of lattice points in the time direction T corresponds to the inverse temperature, $T \sim \beta$. We will refer to temperature as β^{-1} throughout this section so as not to confuse it with T, the width of the time direction in lattice units. We would like to run our simulations at a spatial size large enough to reach the infinite volume limit so that we can be sure that our results are not dominated by finite-size effects.

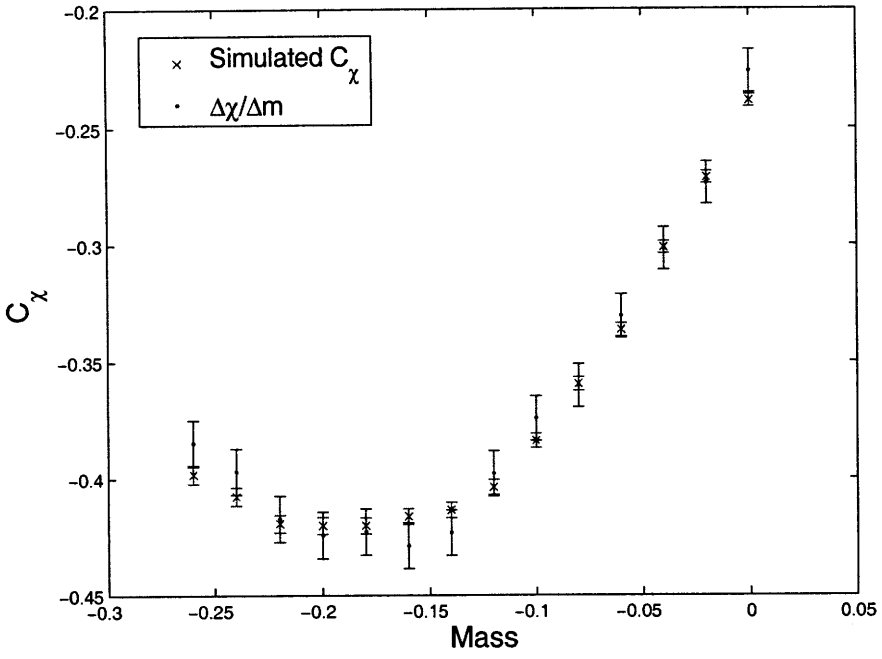

Figure 5-5: Mass susceptibility of two interacting Majorana fermions ($g^2 = 0.1$) on an 8×8 lattice calculated directly from simulations and by taking the numerical derivative of the condensate.

We want to be simulating in the infinite volume limit, which means that we want

$$L\Lambda \gg 1 \tag{5.4.1}$$

where L/a is the length of the lattice in the spatial direction in lattice units and $a\Lambda$ is the energy scale of our theory. We know from [8] that $a\Lambda$ scales with the coupling and the number of fermion flavors as

$$a\Lambda = \exp\left(-\frac{\pi}{\frac{N}{2}-1}\frac{1}{g^2}\right) \tag{5.4.2}$$

so for a fixed N and L, we can determine the value of g^2 we need to produce the correct energy scale. We will only see full chiral symmetry restoration at the critical mass m_c, so we would like to be simulating as close to m_c as possible. The value of

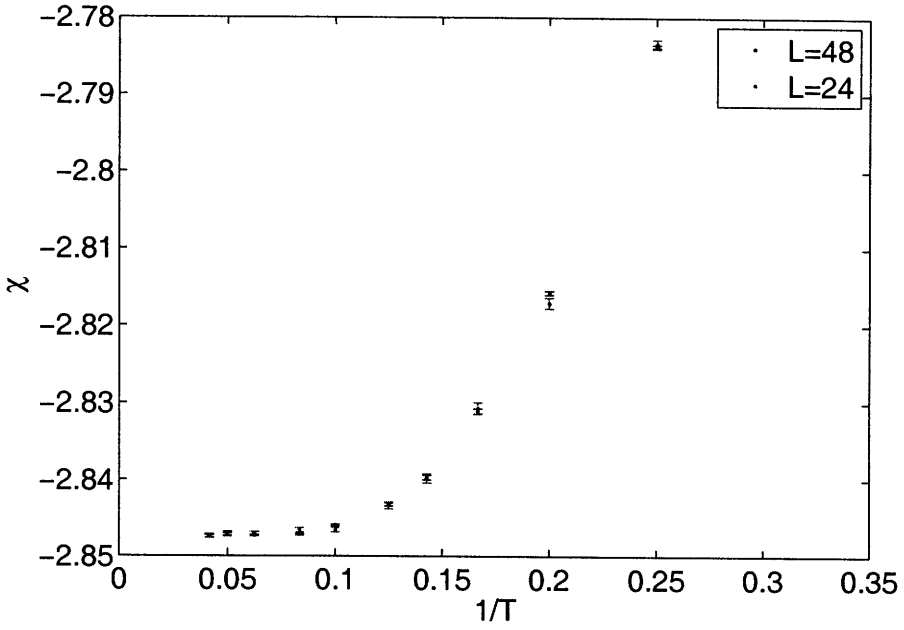

Figure 5-6: Chiral condensate for $L = 24$ and $L = 48$ lattices with $N = 8, g^2 = 0.5$, and $m = -0.5775$. T is the number of lattice points in the time direction, and increasing $1/T$ corresponds to increasing temperature.

the critical mass is a function of both N and g and is given by

$$am_c = -\left(\frac{N}{2} - 1\right) Kg^2 + O(g^4) \tag{5.4.3}$$

where $K = 0.385$ is a constant [12]. Once we have determined a value for g^2, we can estimate am_c, the value of the critical mass in dimensionless lattice units, using equation (5.4.3).

In order to test whether we have achieved the infinite volume limit, we simulate fermions with lattices of two spatial sizes, $L = 24$ and $L = 48$, and varying widths in the time direction: $T = 4, 5, 6, 7, 8, 10, 12, 16, 20, 24$. We compare measurements of the condensate as a function of $1/T$, which corresponds to increasing temperature, for these two spatial sizes. For 8 fermions, at a g^2 of 0.5, from equation (5.4.2), $a\Lambda \approx 0.12$, which means the condition of equation (5.4.1) holds for $L = 48$. The value of the critical mass for $N = 8$ and $g^2 = 0.5$ can be calculated from equation (5.4.3) and is approximately $m_c = -0.5775$. The results are at fixed $N = 8$, $g^2 = 0.5$,

and $m_c = -0.5775$ and are shown in Figure 5-6. We see that the values for χ for $L = 24$ and $L = 48$ sized lattices are within errors of each other for each value of β^{-1} tested. From this plot, we can conclude that we have reached the infinite volume limit at $L = 24$ for the values of N, g, and m we have tested, since doubling the length of the spatial direction does not affect the calculations of χ. The shape of the plot in Figure 5-6 is probably due to lattice effects, as simulations at $g = m = 0$ on the same lattice sizes produce the same shaped plot.

In § 1.3 we learned that for any finite N flavors of $1+1$ dimensional Gross-Neveu fermions, $T_c = 0$. That is, for any $T > 0$, there should be no spontaneous breaking of chiral symmetry. However, from [6] we also know that chiral symmetry is restored at any nonzero T due to the condensation of kinks in the spatial direction. The size of the segments in the spatial direction which are separated by kinks scales with the number of fermion flavors as $\exp(\alpha m_f N/T)$ [6] where α is a constant of $O(1)$ and m_f is the fermion physical mass. Therefore, on a finite lattice of spatial width L, we should expect to observe spontaneous chiral symmetry breaking at low T at large enough N, when the size of the segment is $O(L)$. Then, as the temperature increases, the segment size decreases, and they eventually disappear. Therefore, we should observe chiral symmetry restoration at a nonzero critical temperature for large enough N.

Now we will use a new method to simulate nonzero temperature. We will manipulate the value of the coupling, as done in [8], which alows us to scan continuously in temperature. Increasing the value of g^2 corresponds to increasing the lattice spacing, making the width of the lattice larger, and the temperature smaller. We will perform simulations on a 6×48 lattice, which we already know to be in the infinite volume limit for eight fermions at $g^2 = 0.5$ and critical mass. We compute χ for both $N = 8$ and $N = 16$ flavors of fermions, and scan around the critical value of g^2, such that equation (5.4.2) is satisfied with $a\Lambda \approx 0.12$. Changing g^2 changes the value of m_c according to equation (5.4.3), so as we scan in g^2, we also calculate $m_c(g^2)$ and simultaneously scan in the value of the mass parameter.

In order to see the fermion phase transition, we must get rid of the additive shift

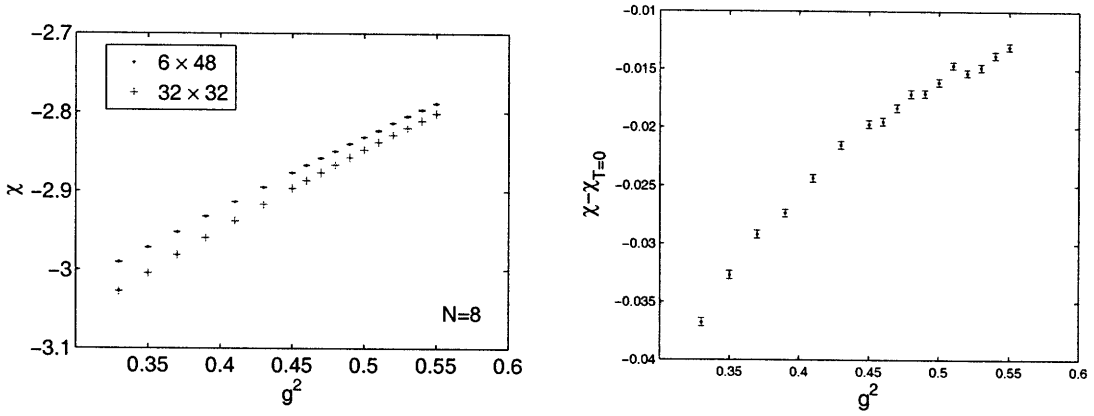

Figure 5-7: Left: χ (computed on a 6×48 lattice) and $\chi_{T=0}$ (computed on a 32×32 lattice) for 8 flavors of fermions as a function of g^2. Increasing g^2 corresponds to decreasing temperature. Right: $\chi - \chi_{T=0}$ for $N = 8$ as a function of g^2.

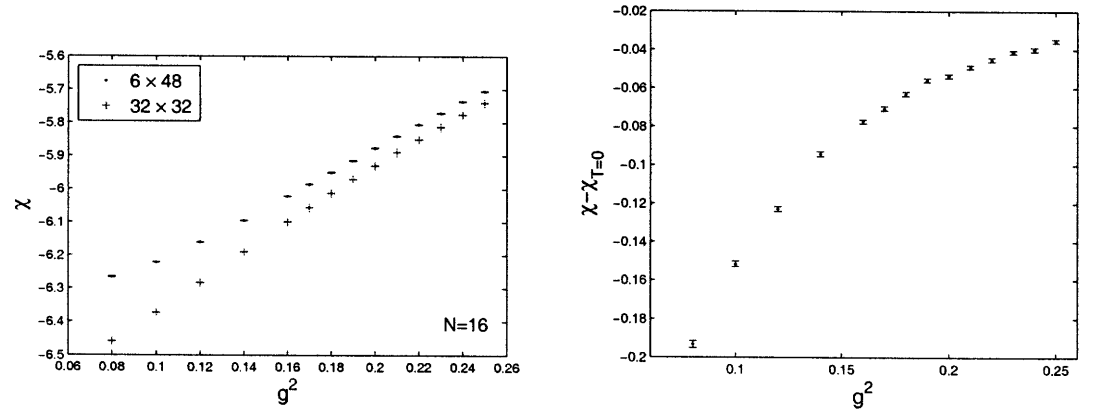

Figure 5-8: Left: χ (computed on a 6×48 lattice) and $\chi_{T=0}$ (computed on a 32×32 lattice) for 16 flavors of fermions as a function of g^2. Increasing g^2 corresponds to decreasing temperature. Right: $\chi - \chi_{T=0}$ for $N = 16$ as a function of g^2.

in χ which arises due to the Wilson lattice discretization. One way to get rid of this shift is by subtracting the zero-temperature value of the condensate, $\chi_{T=0}$, from the value of the condensate at nonzero temperature, $\chi_{T>0}$. We can compute the zero temperature value of χ by performing simulations on a square lattice. From Figure 5-6, we see that we are already in the infinite volume limit at $L = 24$ for $N = 8$ and $g^2 = 0.5$. To make sure we are still sufficiently within this limit, we will simulate fermions at zero temperature on a 32×32 square lattice and calculate $\chi_{T=0}$. Then we will subtract these values from the nonzero temperature calculations of χ done on a 6×48 lattice in order to get rid of the additive shift in the condensate. What we expect to see is the difference in the condensate $\chi - \chi_{T=0}$ approach zero as g^2 increases (decreasing temperature). At low temperature (high g^2) we still expect the chiral symmetry to be broken, so $\chi - \chi_{T=0}$ should be small. However, at high temperature (low g^2), the chiral symmetry should be restored, so χ should differ significantly from its zero temperature value and the magnitude of $\chi - \chi_{T=0}$ should be large. In the large N limit, we expect a second order phase transition to occur at some critical value of the coupling, g_c^2, corresponding to a critical temperature T_c, which depends on N. The transition should be more sharply defined for larger N, and $T_c/\Lambda \rightarrow$ constant for $N \rightarrow \infty$.

We report our results for $N = 8$ in Figure 5-7 and $N = 16$ in Figure 5-8. Both the curve for $N = 8$ and $N = 16$ approach zero at high g^2 as we would expect. However, the change in $\chi - \chi_{T=0}$ over the range of g^2 for $N = 8$ is minimal, whereas it is an order of magnitude for $N = 16$. In addition, the plot of $\chi - \chi_{T=0}$ on the right hand panel of Figure 5-8 for $N = 16$ is more sharply curved than that of Figure 5-7 for $N = 8$. This is consistent with the expectation that a cusp will develop as $N \rightarrow \infty$, as for a second order phase transition in the large N limit.

Chapter 6

Conclusions

We have developed and implemented an efficient cluster algorithm to study the thermodynamic properties of fermions on a lattice. We have reproduced the algorithm of [1] and verified it for free fermions in $1+1$ dimensions. In addition, we have extended this algorithm to the Gross-Neveu model for the first time and computed correlation functions for interacting fermions. Finally, we have studied fermions at nonzero temperature using a cluster algorithm for the first time and produced first results consistent with the expectation of a fermion phase transition for large N.

Because the algorithm we have developed is much more efficient than previously used local updating algorithms, we now have the ability to study Gross-Neveu fermions at increasingly larger lattice sizes and with higher N. Doing this will allow us to observe properties of fermion correlation functions and the chiral phase transition more sharply. We can also extend our calculations to spatially larger lattice sizes, where we eventually expect to see the disappearance of chiral symmetry breaking as $L \gg$ size of the broken symmetry segments. This type of algorithm could also be developed for fermions at a nonzero chemical potential, which would allow us to efficiently study additional interesting thermodynamic properties of interacting fermions in $1+1$ dimensions.

Bibliography

[1] Ulli Wolff. Cluster simulation of relativistic fermions in two space-time dimensions. *Nuclear Physics B*, 789:258–276, 2008.

[2] Christof Gattringer. Loop representation for 2-d wilson lattice fermions in a scalar background field. *Nuclear Physics B*, 543(1-2):533–542, March 1998.

[3] Robert H. Swendsen and Jian-Sheng Wang. Nonuniversal critical dynamics in monte carlo simulations. *Physical Review Letters*, 58(2):86–88, January 1987.

[4] Ulli Wolff. Collective monte carlo updating for spins systems. *Physical Review Letters*, 62(4):361–364, January 1989.

[5] David J. Gross and André Neveu. Dynamical symmetry breaking in asymptotically free field theories. *Physical Review D*, 10(10):3235–3253, November 1974.

[6] Roger F. Dashen, Shang keng Ma, and R. Rajaraman. Finite-temperature behavior of a relativistic field theory with dynamical symmetry breaking. *Physical Review D*, 11(6):1499–1508, March 1975.

[7] Ulli Wolff. The phase diagram of the infinite-n gross-neveu model at finite temperature and chemical potential. *Physics Letters*, 157B(4):303–308, July 1985.

[8] F. Karsch, J. Kogut, and H. W. Wyld. The gross-neveu model at finite temperature and density. *Nuclear Physics B*, 280:289–303, 1987.

[9] Ulli Wolff. Monte carlo errors with less errors. *Computer Physics Communications*, 156(2):143–153, January 2004.

[10] Christof Gattringer, Verena Hermann, and Markus Limmer. Fermion-loop simulation of the lattice gross-neveu model. *Physical Review D*, 76, July 2007.

[11] Verena Hermann. Monte carlo simulation of the gross-neveu model in a fermion loop representation. Master's thesis, Universität Regensburg, 2006.

[12] Tomasz Korzec and Ulli Wolff. Gross-neveu model as a laboratory for fermion discretization. In *PoS Lattice*, 2005.